Active sites in heterogeneous ice nucleation - the example of K-rich feldspars

Authors: Alexei Kiselev[1]*, Felix Bachmann[1,3†], Philipp Pedevilla[4], Stephen J. Cox[4], Angelos Michaelides[5], Dagmar Gerthsen[3] and Thomas Leisner[1,2]

Affiliations:

[1]Atmospheric Aerosol Research Department, Institute for Meteorology and Climate Research, Karlsruhe Institute of Technology (KIT), Hermann-von-Helmholtz Platz 1, 76344 Eggenstein-Leopoldshafen, Germany

[2]Institut für Umweltphysik, Universität Heidelberg, Im Neuenheimer Feld 229, Heidelberg, Germany

[3]Laboratory for Electron Microscopy, Karlsruhe Institute of Technology (KIT), Engesserstrasse 7, 76131 Karlsruhe, Germany

[4]London Centre for Nanotechnology, Thomas Young Centre, and Department of Chemistry, University College London, 17-19 Gordon Street, London, WC1H 0AH, London, UK

[5]London Centre for Nanotechnology, Thomas Young Centre, and Department of Physics and Astronomy, University College London, 17-19 Gordon Street, London, WC1H 0AH, London, UK

*Correspondence to: alexei.kiselev@kit.edu

† Now at Max Planck Institute of Colloids and Interfaces, Am Mühlenberg 1, 14476 Potsdam, Germany

Ice formation on aerosol particles is a process of crucial importance to Earth's climate and the environmental sciences but it is not understood at the molecular level. This is so partly because the nature of active sites, local surface features where ice growth commences, is still unclear. Here we report direct electron-microscopic observations of deposition growth of aligned ice crystals on feldspar, an atmospherically important component of mineral dust. Our molecular-scale computer simulations indicate that this alignment arises from the preferential nucleation of prismatic crystal planes of ice on high-energy (100) surface planes of feldspar. The microscopic patches of (100) surface, exposed at surface defects such as steps, cracks, and cavities, are thought to be responsible for the high ice nucleation efficacy of K-feldspar particles.

One Sentence Summary: Electron microscopy and computer simulations have been used to understand how ice forms on feldspar, the most active component of atmospheric mineral dust.

The freezing of water is one of the most common everyday processes, and hence is of relevance to an enormous number of technological and environmental phenomena. For example, ice formation is at the heart of precipitation formation in the majority of clouds, and therefore influences freshwater distribution. When water freezes it does so in a heterogeneous process facilitated by the presence of foreign ice nucleating (IN) particles. A wide variety of materials have been shown to be effective in promoting ice nucleation (see e.g. Wilson et al. (*1*), Atkinson et al. (*2*), Hiranuma et al. (*3*)), with mineral dust being the most abundant IN particle type in Earth's atmosphere (*4*, *5*). However, the ice nucleating efficacy of mineral dust (and other materials) varies by several orders of magnitude and the question of what property (or combination of properties) is responsible for any particular mineral dust aerosol being a bad or good IN particle is still under debate (*4*, *6–10*).

Although there has been a considerable body of work aimed at understanding the structure of water and ice at interfaces, this has generally not provided detailed information about the mechanism of ice formation (*11*, *12*). In the absence of mechanistic insight, the IN efficacy of mineral dust solid particles is generally characterized by the surface density of ice nucleating active sites (*13*, *14*), an empirical parameter relating the apparent number of IN events to temperature and particle size (*15*). From previous experimental and modelling studies, several factors responsible for high IN efficacy of particles have been suggested (*4*, *16–20*): crystal lattice match allowing for epitaxial growth of ice (*21–26*), surface hydroxyl groups increasing the chemical affinity to ice (*17*, *19*, *27–31*), and surface defects (such as steps, cracks, and cavities) which locally enhance the density of adsorbed water molecules (*13*, *32*, *33*) or reduce their surface diffusivity (*17*, *34*). The importance of defects has been demonstrated in experiments where substrates with excellent lattice match to ice (such as silver iodide) could be made yet more effective in nucleating ice through the introduction of surface morphological irregularities (*35*,

36). Recent molecular-scale simulations, however, question the importance of lattice match and show that the connection with hydrophobicity can be extremely complex (*20*, *27*, *29*, *31*, *37–39*).

Due to the lack of direct experimental evidence, it remains unclear which of the above factors plays a dominant role in regulating the IN properties of specific substrates. To better address this issue we have performed an extensive set of experimental and modelling studies of ice nucleation on K-rich feldspar. The focus in the current study is primarily on ice nucleation from water vapor (i.e. deposition mode nucleation) at cold temperatures (233 - 248 K). We have chosen feldspar because it has recently been identified as one of the most active atmospherically relevant ice nucleating minerals (*2*, *10*). The specific feldspar samples examined in our experiments were orthoclase from Michigan, USA (FSM) and microcline from the Mt. Maloso region, Malawi (FS04) (for more information on these samples see recent work of Peckhaus et al. (*40*)). On the basis of environmental scanning electron microscopy (ESEM) measurements we find that ice crystals grow in a very specific manner, with the nucleation originating at defect sites of the substrate. From these high resolution observations and molecular modelling, we conclude that the defective regions expose microscopic patches of (100) surfaces and it is at these patches that ice grows along it's prismatic face. Such (100) surfaces are not expressed as macroscopic surfaces of feldspar particles (i.e. they are not part of the equilibrium crystal shape of feldspar particles and are not produced by cleavage or environmental mechanical processing) but may be present microscopically at defective regions arising during natural weathering. This work therefore unravels the nature of the active sites in ice nucleation on feldspar and opens up a new paradigm for the mechanism of heterogeneous ice nucleation, wherein facets with relatively high surface free energy play a leading role.

ESEM observations of ice nucleation

K-Feldspar ($KAlSi_3O_8$) is a rock-forming framework silicate mineral. It has two crystallographic planes that lead to "perfect" (001) and "good" (010) cleavage (Fig. 1a). Even though a feldspar (001) surface is said to cleave perfectly, when prepared by mechanical splitting and examined in microscopic detail it is far from being atomically smooth. It exposes a vast array of topographic features such as steps, cavities and kinks, (see Fig. 2A and Fig. S2 of the Supplementary Material). This surface complexity thus makes it ideal for studying ice nucleating active sites.

We observe the nucleation and growth of ice on feldspar samples mounted on a cooled specimen holder in an environmental scanning electron microscope ESEM operating in an atmosphere of controlled relative humidity well below water saturation (see Supplementary Materials for details). In Fig 2 we show results from an experiment involving a number of ice nucleation-evaporation cycles on the (001) face of the FSM sample at 233 K (a movie 'SM01.mp4' is available in the Supplemental Material). We find that ice invariably nucleates in the vicinity of defect sites such as steps, cracks and inside cavities. This is particularly apparent by comparing Figs. 2A and 2B, where in Fig. 2A the sites of ice nucleation are indicated. Specifically, in Fig. 2A the sites of ice nucleation are mapped onto the image of the bare feldspar specimen and they are color coded according to the time at which they appear. It is obvious that nucleation sites cluster near the surface defects and in every nucleation cycle the first ice crystal (the largest hexagonal prism in Fig. 2B) always appeared in a cavity (shown by the red arrow in Fig. 2A, see also movie 'SM04.mp4'). We note that preferential nucleation of ice in the vicinity of defects occurs irrespective of the origin, the weathering procedure, or whether or not any chemical treatment was applied to the specimens (for details see the Supplementary Materials).

A key observation reported in this study is the almost perfect orientation of pristine ice crystals nucleating on K-rich feldspar throughout the atmospherically relevant temperature range from 248 K to 233 K. This striking feature is already visible in Fig. 2B but shown in more detail in Fig. 3 and in the movies available in SM. The orientation of ice crystals is identical with respect to a) the inclination of the c-axis of ice to the (001) face of feldspar, and b) the rotational orientation of the ice crystals about their c-axis (compare Fig. 1B for illustration of the crystallographic planes and axes of hexagonal ice I_h). Out of over 300 individual ice crystals observed in this study, 80% have an identical orientation on the FSM specimen and 85% on the FS04 specimen. The average fraction of aligned crystals within each individual nucleation experiment was 90%. Most importantly, the crystals exhibit the same orientation independent of whether they were nucleating on the (001) or (010) crystal faces of feldspar (see Fig. 3A and movie 'SM03.mp4' in SM), implying that nucleation sites responsible for the orientation and alignment of the ice crystals are exposed in surface defects on both, the (001) and (010) surfaces. This observation also suggests that contaminants on the surface (either chemical or biological in nature) are very unlikely to be responsible for ice nucleation, as they would have to coat the entire feldspar specimen and its different facets in a similar manner. In cases where multiple faces of the specimen were observed simultaneously, we could confirm that the nucleation on both the (001) and (010) surfaces occurred at very similar values of ice super-saturation (Fig. S4).

From numerous experiments under different conditions (as outlined in the Supplementary Materials) we find that monocrystalline ice crystals grow in the same orientation when the following circumstances are fulfilled: a) The K-feldspar specimen had been aged, either naturally (exposed to lab air for at least a day) or in carbonated water; b) the cooling rate does not exceed 2 K/min (to ensure the diffusion limited growth of ice crystal); and c) the onset temperature of ice

nucleation is above 230 K. All three of these conditions are relevant for the deposition nucleation of ice on atmospheric mineral dust particles.

Under favorable observation conditions, the inclination of the ice crystals with respect to feldspar could be measured. In particular, as shown in Fig. 4, the (010) face of feldspar is lying in the image plane, and the c-axis of the ice crystal is inclined by 116° with respect to the (001) feldspar face. This matches the angle β=116.03° between the (001) and (100) crystallographic planes in ideal orthoclase feldspar (*41*) (Fig. 1A) and corresponds to perfect alignment of the c-axes of feldspar and ice. In addition, all ice crystals showing this alignment have one of their prismatic axes (a_1…a_3, c.f. Fig. 1B) parallel to the b-axis of feldspar. These observations suggest that the orientation of the nucleated ice crystals is governed by the crystalline structure of the underlying feldspar sample. The observed match of the two lattice orientations can be explained by the ice crystal nucleating with its primary prism plane $(10\bar{1}0)$ on the (100) crystallographic plane of feldspar (see Fig. 1 for crystallographic planes of feldspar and ice).

Due to its high surface energy and associated fast growth rate from the melt, the (100) plane in feldspar rarely appears as a free growing crystal face in natural macroscopic feldspar specimens (*41*). Tiny patches of this plane, however, will appear at steps and in cavities on both cleavage faces as a result of mechanical fracture or weathering. Panels A) to E) in Figure 4 give direct evidence that this is indeed the case. Here a magnified image of a cavity in the (010) face of FSM with an ice crystal nucleating on one of the walls is shown. The plane of the wall is aligned with the (100) crystal plane, as shown by the projection of the orthoclase unit cell (yellow) matching the crystal lattice of the specimen. Already at the earliest stage of growth ($t < 2$ s after nucleation, Fig. 4B) the ice crystal (indicated by the arrow) exhibits a preferential orientation consistent with the nucleation of its prism face on the (100) patch in feldspar. This orientation becomes obvious with further growth, when several other crystals appear on both faces of feldspar

in the same orientation (t > 30 s, Fig. 4E). Fig. 4F illustrates how the nucleation of ice from the $(10\bar{1}0)$ plane on a step with (100) orientation explains the identical orientation of ice crystals on both (001) and (010) faces of feldspar. The relative positions and orientation of ice crystals in Fig. 4F corresponds to the case shown in Fig. 4E. The preferential ice orientation combined with the fact that ice always seems to grow at defect sites where (100) patches may be exposed suggests these patches are the ice nucleating active sites.

Note that at the early growth stage (t = 10 s, Fig. 4D) the crystal shape is not a hexagonal column but exhibit the true equilibrium growth habit of ice (*42*). In equilibrium, all crystallographic faces of ice (basal, prism and pyramidal) grow with the same linear velocity. As the crystal becomes larger, the growth of basal and prism faces slows down and the pyramidal faces become less pronounced.

Atomistic simulations of feldspar-ice interface

Recently some of us have shown on the basis of atomistic computer simulations that a stable ice-like structure can form on the most easily cleaved (001) surface of feldspar (*43*). In comparison to (001) the structure of the (100) surface of microcline is fairly complex with a ca. 13×7 Å surface unit cell. In addition, in a wet environment under-coordinated atoms arising from the cleavage of the surface will be terminated with hydroxyl groups (aluminol (Al-OH) and silanol (Si-OH)) (*41*, *44–46*). Given the complex structure of the feldspar (100) surface, it is not clear if ice can form stable structures on top of it. To address this issue we carried out an extensive set of atomistic computer simulations in which we searched for stable ice-like structures at the feldspar (100) surface, based on the ClayFF force field (*47*) to represent feldspar and the SPC model to represent water (*48*). For comparison we also searched for structures on the feldspar (010) and (110) surfaces, since the observed relative orientation of crystal habits of feldspar and ice can in principle

be explained by ice growth from secondary prismatic planes on these surfaces (see SM for more detail). A very broad range of ice structures was considered and the main result is shown in Fig. 5, where we present an atomistic model of the feldspar (100) - ice interface. Interestingly, we do indeed find that the stable face of ice on the feldspar (100) surface is the primary prismatic plane $(10\bar{1}0)$ (with an adsorption energy of -0.58 eV/H_2O, for further details see SM). The prism plane is favored over the basal face because the rectangular symmetry of the former matches that of the underlying substrate fairly well, enabling for a 3×1 array of prism face unit cells to fit within one unit cell of the feldspar (100) surface. In fact, the fit between the prism face and the feldspar (100) surface is particularly good, with very little strain within the overlayer. This can be seen, for example, by measuring the median O-O (2.74 Å) distances and O-O-O (109.4°) angles within the ice overlayer. On average these values are within 0.01 Å and 0.1° of the corresponding values in the SPC model of bulk ice, using an equivalent computational set-up. None of the other ice-like structures identified on the (100) surface or the other feldspar surfaces yielded ice with as little strain as this feldspar (100) / ice $(10\bar{1}0)$ interface.

Two aspects of the results are worth elaborating on in more detail. First, contrary to the often implicitly made assumption that in the case of epitaxial growth ice nucleates from the basal face, our results suggest that this does not happen on K-feldspar. Basal plane epitaxy was most often observed in the experiments with synthetic and natural substrates (*21*, *22*, *49*). However, nucleation of the prism plane on a substrate is not unknown (*21*). Several MD studies have also found nucleation of a prism face aligned with the basal face of clay minerals (*19*, *31*).

Second, as shown in Fig. 5, the interaction between feldspar and water is indeed mediated by hydroxyl groups on the feldspar surface. The prism face grows directly on the hydroxylated (100) feldspar surface, in contrast to the predictions of ice growth on the (001) surface where a non-ice-like layer mediates the structure between ice and the substrate (*43*). This suggests that

surface OH groups play an important role in the ice nucleation process, by allowing ice-like structures to form even without an apparent epitaxial match. Thus, it is not surprising, that affecting the OH arrangement by natural weathering or chemical treatment impacts the ice nucleation process, as discussed further in the SM. The role of OH groups might provide a clue for understanding the observed strong variability of ice nucleation efficacies of various feldspars (*10*, *40*) since the natural variability of lattice constants, microtexture, heterogeneity of Al:Si ratio etc., will be reflected in the ordering of the surface hydroxyl groups thus affecting the ability of feldspar dust particles to serve as ice nucleating particles.

We hypothesize that the affinity of feldspar (100) patches to ice, discovered in this study, should be universal for both, deposition and immersion, modes of heterogeneous ice nucleation. In both regimes, the property of the active site to reduce the energy of nucleus formation defines the ice nucleation efficiency of a substrate. In both regimes, the energy of the nucleus-substrate interface must be the same. What is different, however, is the flux of water molecules towards the critical nucleus, surface tension of the nucleus, and therefore its size. We argue that the property of (100) surface patch to bind a certain crystal plane of ice (prism) should be relevant in immersion freezing as well as in deposition ice nucleation, leading to acceleration of nucleation rate. The ice nucleation onset conditions, as well as the observable features (habit and orientation of ice crystals) will, of course, be different for different nucleation modes.

Conclusions

In summary, we have experimentally identified the ice nucleating active sites on the surface of K-rich feldspar as the surface patches with (100) crystallographic orientation. These patches occur exclusively at surface features like steps, cracks and cavities which arise during fracturing processes (such as grinding or mechanical weathering). The preferential nucleation of ice on the

defects is dominated by the presence of these patches. This finding will help to characterize the IN properties of natural mineral dust aerosol particles which almost universally contain feldspar. The feldspar particles with the highest density of specific crystal planes exposed in the surface defects should constitute the most efficient ice nucleating particles. Moreover, aided by atomistic computer simulations we were able to show, that on these patches hydroxyl groups mediate the interaction between ice and feldspar. To our knowledge, these observations constitute the first direct identification of an ice nucleating surface site on an inorganic substrate at the molecular level. The nucleation of non-basal faces of ice on surfaces with relatively high surface free energy, which are not expressed as dominant surface facets, could be relevant to ice formation on other mineral dusts and substrates.

Acknowledgements

The preparation and XRD characterization of feldspar samples at the Institute of Applied Geosciences of TU Darmstadt (Dr. Martin Ebert) as a part of cooperation within the DFG-funded research unit INUIT (DFG-FOR-1525-6343) is greatly acknowledged. This work was also partly supported by KIT Startup Budget 2011 (2066992441-Start-Up-Eisbildung-ESEM GG 507). A.K and F. B. would like to thank Volker Zibat (KIT LEM) and Jens Nadolny (KIT IMK-AAF) for technical and programming support. A. M. is supported by the European Research Council under the European Union's Seventh Framework Programme (FP/2007-2013) / ERC Grant Agreement number 616121 (HeteroIce project). A. M. is also supported by the Royal Society through a Royal Society Wolfson Research Merit Award. P. P. and A. M. are grateful for computational resources provided by the Materials Chemistry Consortium through the EPSRC grant number EP/L000202, UCL Research Computing and the London Centre for Nanotechnology. A. K. and T. L. are

supported by the Helmholtz Association under Atmosphere and Climate Programme (ATMO). D.G. and F.B. were supported by the Karlsruhe Institute of Technology.

The experimental and computational datasets used in this work are available as a supplementary online material.

References

1. T. W. Wilson *et al.*, A marine biogenic source of atmospheric ice-nucleating particles. *Nature*. **525**, 234–238 (2015).
2. J. D. Atkinson *et al.*, The importance of feldspar for ice nucleation by mineral dust in mixed-phase clouds. *Nature*. **498**, 355–8 (2013).
3. N. Hiranuma *et al.*, Ice nucleation by cellulose and its potential contribution to ice formation in clouds. *Nat. Geosci.* **8**, 273–277 (2015).
4. M. A. Freedman, Potential Sites for Ice Nucleation on Aluminosilicate Clay Minerals and Related Materials. *J. Phys. Chem. Lett.* **6**, 3850–3858 (2015).
5. N. Hiranuma *et al.*, A comprehensive parameterization of heterogeneous ice nucleation of dust surrogate: laboratory study with hematite particles and its application to atmospheric models. *Atmos. Chem. Phys.* **14**, 13145–13158 (2014).
6. C. Hoose, O. Möhler, Heterogeneous ice nucleation on atmospheric aerosols: a review of results from laboratory experiments. *Atmos. Chem. Phys.* **12**, 9817–9854 (2012).
7. B. J. Murray, D. O'Sullivan, J. D. Atkinson, M. E. Webb, Ice nucleation by particles immersed in supercooled cloud droplets. *Chem. Soc. Rev.* **41**, 6519 (2012).
8. J. D. Yakobi-Hancock, L. A. Ladino, J. P. D. Abbatt, Feldspar minerals as efficient deposition ice nuclei. *Atmos. Chem. Phys.* **13**, 11175–11185 (2013).
9. G. P. Schill, K. Genareau, M. A. Tolbert, Deposition and immersion-mode nucleation of ice by three distinct samples of volcanic ash. *Atmos. Chem. Phys.* **15**, 7523–7536 (2015).
10. A. D. Harrison *et al.*, Not all feldspar is equal: a survey of ice nucleating properties across the feldspar group of minerals. *Atmos. Chem. Phys.* **16**, 10927–10940 (2016).
11. A. Hodgson, S. Haq, Water adsorption and the wetting of metal surfaces. *Surf. Sci. Rep.* **64**, 381–451 (2009).
12. J. Carrasco, A. Hodgson, A. Michaelides, A molecular perspective of water at metal interfaces. *Nat. Mater.* **11**, 667–674 (2012).
13. N. H. Fletcher, Active Sites and Ice Crystal Nucleation. *J. Atmos. Sci.* **26**, 1266–1271 (1969).
14. N. H. Fletcher, Nucleation and Growth of Ice Crystals Upon Crystalline Substrates. *Aust. J. Phys.* **13**, 408 (1960).

15. P. J. Connolly *et al.*, Studies of heterogeneous freezing by three different desert dust samples. *Atmos. Chem. Phys.* **9**, 2805–2824 (2009).

16. W. Cantrell, A. Heymsfield, Production of Ice in Tropospheric Clouds: A Review. *Bull. Am. Meteorol. Soc.* **86**, 795–807 (2005).

17. H. R. Pruppacher, J. D. Klett, *Microphysics of clouds and precipitation* (Kluwer Academic Publishers, 2nd rev. a., 2004).

18. G. Vali, Ice Nucleation Theory. *Molecules*. **1999**, 1–22 (1999).

19. S. J. Cox, Z. Raza, S. M. Kathmann, B. Slater, A. Michaelides, The microscopic features of heterogeneous ice nucleation may affect the macroscopic morphology of atmospheric ice crystals. *Faraday Discuss.* **167**, 389 (2013).

20. M. Fitzner, G. C. Sosso, S. J. Cox, A. Michaelides, The Many Faces of Heterogeneous Ice Nucleation: Interplay between Surface Morphology and Hydrophobicity. *J. Am. Chem. Soc.* **137**, 13658–13669 (2015).

21. G. W. Bryant, J. Hallett, B. J. Mason, The epitaxial growth of ice on single-crystalline substrates. *J. Phys. Chem. Solids*. **12**, 189–IN18 (1959).

22. J. L. Caslavsky, K. Vedam, Epitaxial growth of ice crystals on the muscovite cleavage plane and their relation to partial dislocations. *J. Appl. Phys.* **42**, 516–520 (1971).

23. N. Cho, J. Hallett, Epitaxial ice crystal growth on covellite (CuS) I. Influence of misfit strain on the growth of non-thickening crystals. *J. Cryst. Growth*. **69**, 317–324 (1984).

24. T. Kobayashi, The Growth of Ice Crystals on Covellite and Lead Iodide Surfaces. *Contrib. from Inst. Low Temp. Sci.* **692**, 1–22 (1965).

25. B. Vonnegut, The nucleation of ice formation by silver iodide. *J. Appl. Phys.* **18**, 593–595 (1947).

26. D. Turnbull, B. Vonnegut, Nucleation Catalysis. *Ind. Eng. Chem.* **44**, 1292–1298 (1952).

27. T. Croteau, a. K. Bertram, G. N. Patey, Adsorption and structure of water on kaolinite surfaces: Possible insight into ice nucleation from grand canonical Monte Carlo calculations. *J. Phys. Chem. A*. **112**, 10708–10712 (2008).

28. T. Croteau, A. K. Bertram, G. N. Patey, Simulation of water adsorption on kaolinite under atmospheric conditions. *J. Phys. Chem. A*. **113**, 7826–7833 (2009).

29. X. L. Hu, A. Michaelides, Ice formation on kaolinite: Lattice match or amphoterism? *Surf. Sci.* **601**, 5378–5381 (2007).

30. X. L. Hu, A. Michaelides, Water on the hydroxylated (0 0 1) surface of kaolinite: From monomer adsorption to a flat 2D wetting layer. *Surf. Sci.* **602**, 960–974 (2008).

31. S. A. Zielke, A. K. Bertram, G. N. Patey, Simulations of Ice Nucleation by Kaolinite (001) with Rigid and Flexible Surfaces. *J. Phys. Chem. B*. **120**, 1726–1734 (2016).

32. H. K. Christenson, Two-step crystal nucleation via capillary condensation. *CrystEngComm*. **15**, 2030 (2013).

33. C. Marcolli, Deposition nucleation viewed as homogeneous or immersion freezing in pores and cavities. *Atmos. Chem. Phys.* **14**, 2071–2104 (2014).

34. V. B. Federer, Ueber den Einfluss der Oberflaecheneigenschaften von Halbleitern auf ihre Eiskeimfaehigkeit. *Z. Angew. Math. Phys*. **19**, 378–390 (1968).

35. J. Hallett, S. K. Shrivastava, Nucleation of supercooled water by large single crystals of silver iodide. *J. Rech. Atmos.* **5**, 223–236 (1973).

36. B. J. Anderson, J. Hallett, Supersaturation and Time Dependence of Ice Nucleation from the Vapor on Single Crystal Substrates. *J. Atmos. Sci.* **33** (1976), pp. 822–832.

37. S. J. Cox, S. M. Kathmann, J. a. Purton, M. J. Gillan, A. Michaelides, Non-hexagonal ice at hexagonal surfaces: the role of lattice mismatch. *Phys. Chem. Chem. Phys.* **14**, 7944 (2012).

38. L. Lupi, V. Molinero, Does Hydrophilicity of Carbon Particles Improve Their Ice Nucleation. *J. Phys. Chem. A* (2014), doi:10.1021/jp4118375.

39. L. Lupi, A. Hudait, V. Molinero, Heterogeneous nucleation of ice on carbon surfaces. *J. Am. Chem. Soc.* **136**, 3156–3164 (2014).

40. A. Peckhaus, A. Kiselev, T. Hiron, M. Ebert, T. Leisner, A comparative study of K-rich and Na/Ca-rich feldspar ice nucleating particles in a nanoliter droplet freezing assay. *Atmos. Chem. Phys.* **16**, 11477–11496 (2016).

41. J. V. Smith, *Feldspar Minerals 2 Chemical and Textural Properties* (Springer Berlin Heidelberg, ed. 1, 1974).

42. K. G. Libbrecht, On the Equilibrium Shape of an Ice Crystal. *Proc. R. Soc. London*. **49**, 323–343 (2012).

43. P. Pedevilla, S. J. Cox, B. Slater, A. Michaelides, Can Ice-Like Structures Form on Non-Ice-Like Substrates? The Example of the K-feldspar Microcline. *J. Phys. Chem. C*. **120**, 6704–6713 (2016).

44. I. Parsons, Ed., *Feldspars and Their Reactions* (Kluwer Academic Publishers, Series C:, 1994), vol. 421.

45. J. V Smith, Atmospheric weathering and silica-coated feldspar: analogy with zeolite molecular sieves, granite weathering, soil formation, ornamental slabs, and ceramics. *Proc. Natl. Acad. Sci. U. S. A.* **95**, 3366–3369 (1998).

46. H. Behrens, An Infrared Spectroscopic Study of Hydrogen Feldspar (HA1Si3O8). *Mineral. Mag.* **59**, 15–24 (1995).

47. R. T. Cygan, J.-J. Liang, A. G. Kalinichev, Molecular Models of Hydroxide, Oxyhydroxide, and Clay Phases and the Development of a General Force Field. *J. Phys. Chem. B*. **108**, 1255–1266 (2004).

48. H. J. C. Berendsen, J. P. M. Postma, W. F. van Gunsteren, J. Hermans, Interaction models for water in relation to protein hydration. *Intermol. Forces*, 331–342 (1981).

49. N. Fukuta, B. . Mason, Epitaxial growth of ice on organic crystals. *J. Phys. Chem. Solids*. **24**, 715–718 (1963).

50. F. Zimmermann *et al.*, Ice nucleation properties of the most abundant mineral dust phases. *J. Geophys. Res.* **113**, D23204 (2008).

51. M. Ebert, M. Inerle-Hof, S. Weinbruch, Environmental scanning electron microscopy as a new technique to determine the hygroscopic behaviour of individual aerosol particles. *Atmos. Environ.* **36**, 5909–5916 (2002).

52. F. Zimmermann, M. Ebert, A. Worringen, L. Schütz, S. Weinbruch, Environmental scanning electron microscopy (ESEM) as a new technique to determine the ice nucleation

capability of individual atmospheric aerosol particles. *Atmos. Environ.* **41**, 8219–8227 (2007).

53. O. J. Schumann, Cologne Laue Indexation Program, (available at http://clip4.sourceforge.net)
54. E. Yokoyama, T. Kuroda, Pattern formation in growth of snow crystals occurring in the surface kinetic process and the diffusion process. *Phys. Rev. A*. **41**, 2038–2049 (1990).
55. K. G. Libbrecht, The physics of snow crystals. *Reports Prog. Phys.* **68**, 855–895 (2005).
56. K. G. Libbrecht, Growth rates of the principal facets of ice between -10C and -40C. *J. Cryst. Growth*. **247**, 530–540 (2003).
57. K. W. Kolasinski, *Surface Science: Foundations of Catalysis and Nanoscience* (John Wiley & Sons, Ltd, Third edit., 2012).
58. P. V. Hobbs, *Ice Physics* (Oxford University Press, New York, 2010).
59. C. Hoose, O. Möhler, Heterogeneous ice nucleation on atmospheric aerosols: a review of results from laboratory experiments. *Atmos. Chem. Phys.* **12**, 9817–9854 (2012).
60. K. G. Libbrecht, A Critical Look at Ice Crystal Growth Data. *eprint arXiv:cond-mat/0411662*, 21 (2004).
61. S. K. Sihvonen *et al.*, Chemical and physical transformations of aluminosilicate clay minerals due to Acid treatment and consequences for heterogeneous ice nucleation. *J. Phys. Chem. A*. **118**, 8787–96 (2014).
62. D. Van Der Spoel *et al.*, GROMACS: fast, flexible, and free. *J. Comput. Chem.* **26**, 1701–1718 (2005).
63. B. Hess, C. Kutzner, D. Van Der Spoel, E. Lindahl, GRGMACS 4: Algorithms for highly efficient, load-balanced, and scalable molecular simulation. *J. Chem. Theory Comput.* **4**, 435–447 (2008).
64. S. Kerisit, C. Liu, E. S. Ilton, Molecular dynamics simulations of the orthoclase (001)- and (010)-water interfaces. *Geochim. Cosmochim. Acta*. **72**, 1481–1497 (2008).

Figure captions

Figure 1. A) The crystal structure and lattice planes of K-feldspar (orthoclase); unit cell angles are $\alpha = 90°$, $\beta = 116.03°$, $\gamma = 90°$; each Si^{4+} (blue) and each Al^{3+} (green) is located in the centre of a tetrahedron with four oxygen atoms in its vertices (not shown). K^+ ions (violet spheres) occupy the framework voids and provide for the neutral electric charge of the bulk mineral structure; B) hexagonal lattice unit of ice I_h showing the basal face (0001) and the family of primary prism planes $(10\bar{1}0)$ (translucent blue).

Figure 2. Heterogeneous ice nucleation on (001) face of feldspar (FSM), weathered in carbonated water. A) Nucleation sites of individual ice crystals in 8 subsequent nucleation-evaporation cycles, plotted over the image of the bare feldspar face. The color code gives the time of nucleation in seconds with respect to the first detected crystal (the color scale bar is on the right). Note the preferential nucleation on steps and cavities. The red arrow shows the site of the first nucleation event repeatedly occurring in all cycles. B) Snapshot of the ice crystals nucleated at 233 K in the first nucleation-evaporation cycle.

Figure 3. Preferential orientation of ice crystals nucleated on the surface of weathered feldspar: A) (010) and (001) surface of FSM at 241 K; B) (001) surface of FS04 at 244 K, side view.

Figure 4. Nucleation of an ice crystal on a patch with (100) orientation at 251 K. Panels A-E: An ice crystal nucleating on the inner wall of a cavity in the (010) face of the FSM specimen (marked with arrow in panel B). The orientation of the wall visually corresponds to the (100) crystal plane of orthoclase. The relative orientation of crystal planes is shown in yellow, with (010) facing up. The specimen stage has not been moved between frames. F) schematic drawing of ice crystals nucleating from their $(01\bar{1}0)$ planes on the steps with (100) orientation (red filled surface and the hidden face of the step on the (010) face of feldspar; the relative position of ice crystals to each other and with respect to crystal faces of feldspar specimen corresponds to the case shown in panel E).

Figure 5. Side (A, B) and normal top (C) views of the most stable structure of ice on feldspar (100) found in force field simulations. Ice I_h is attached with its primary prism plane $(10\bar{1}0)$ to the (100) face of feldspar. Colors of tetrahedra are the same as in Fig. 1. Oxygen and hydrogen atoms in ice are shown in red and grey respectively. In the top view (panel c), the feldspar underlying structure is shown in pale colors. The primitive feldspar (100) slab unit cell (orthogonal) used in the simulations is shown as the open red box, whereas the axes show the directional vectors of an ideal monoclinic feldspar unit cell.

Supplementary Materials:

Author contributions

Materials and Methods

Supplementary Text

Figures S1-S9

Table S1

Movies S1-S4

Supplementary References (*50* - *64*)

GROMACS structure file of ice on feldspar (100)

Experimental dataset: zipped folder that contains the original experimental data: ice crystal nucleation map with crystal coordinates from eight nucleation cycles, data used for calculation of the on-set supersaturation, wireframes of crystal habits, and original image frames for all figures and supplementary figures recorded with the ESEM.

Computational dataset: zipped folder that contains all of our main structures as well as files that contain information about the computational settings used in this work.

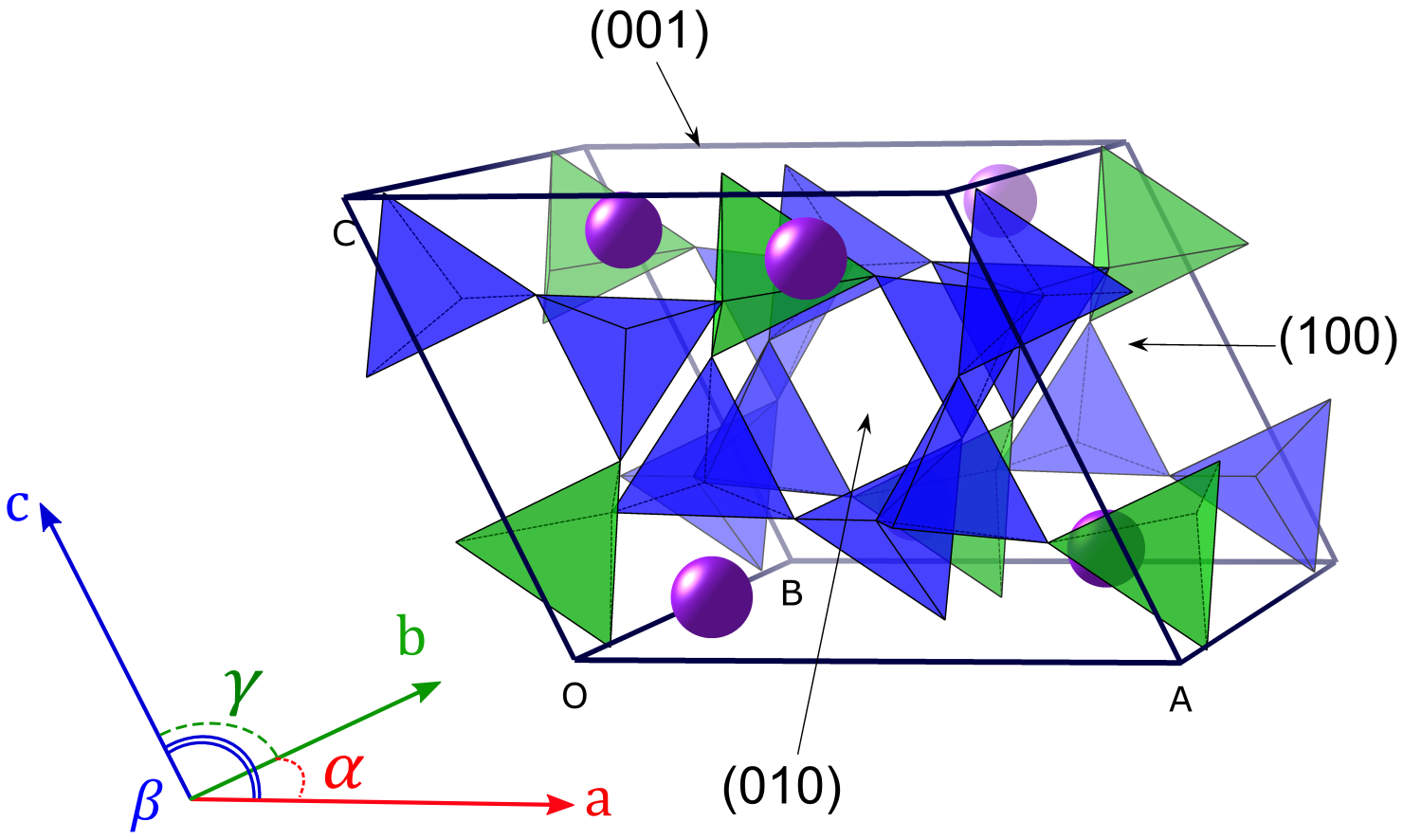

Figure 1A

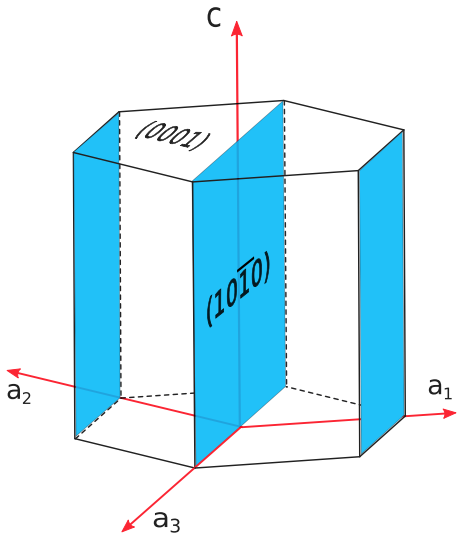

Figure 1B

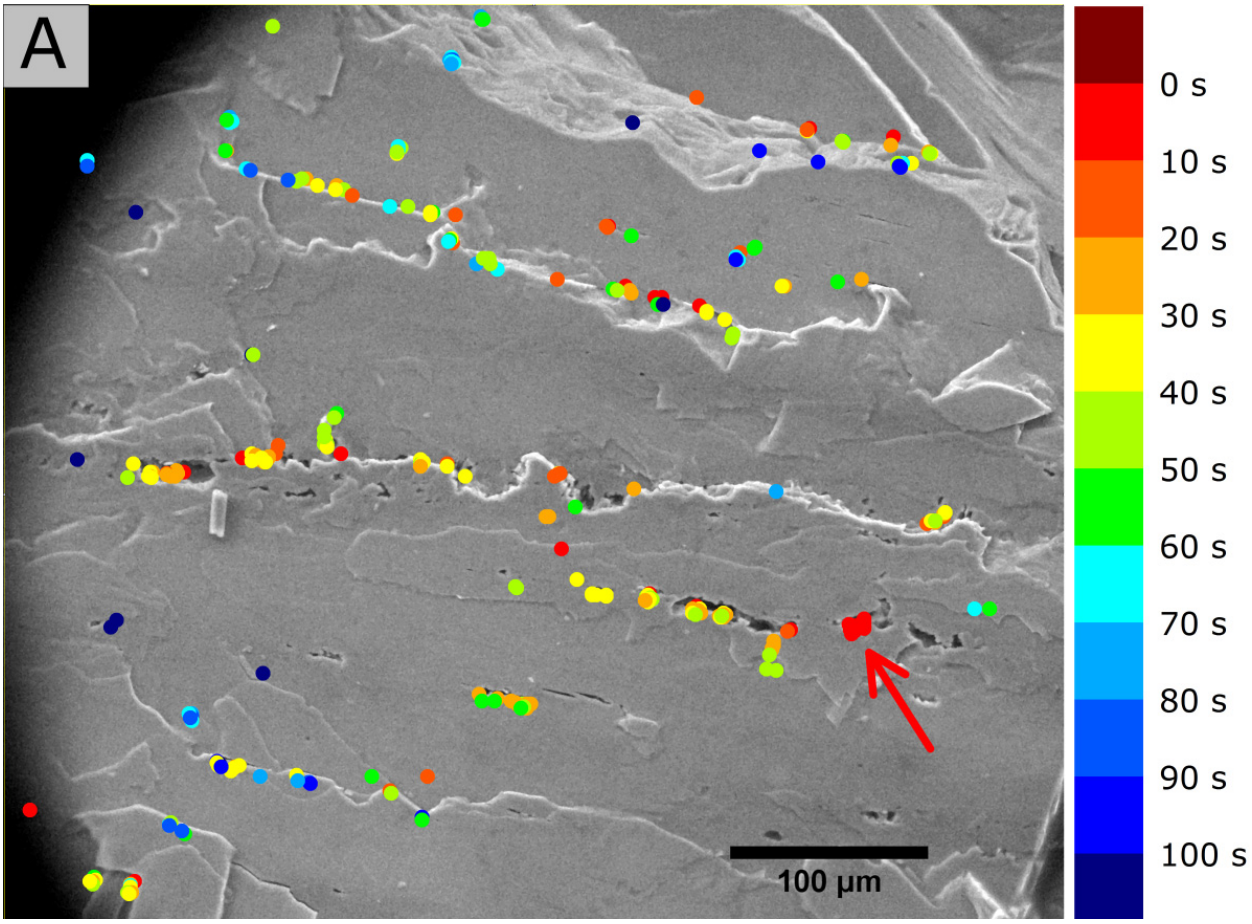

Figure 2A

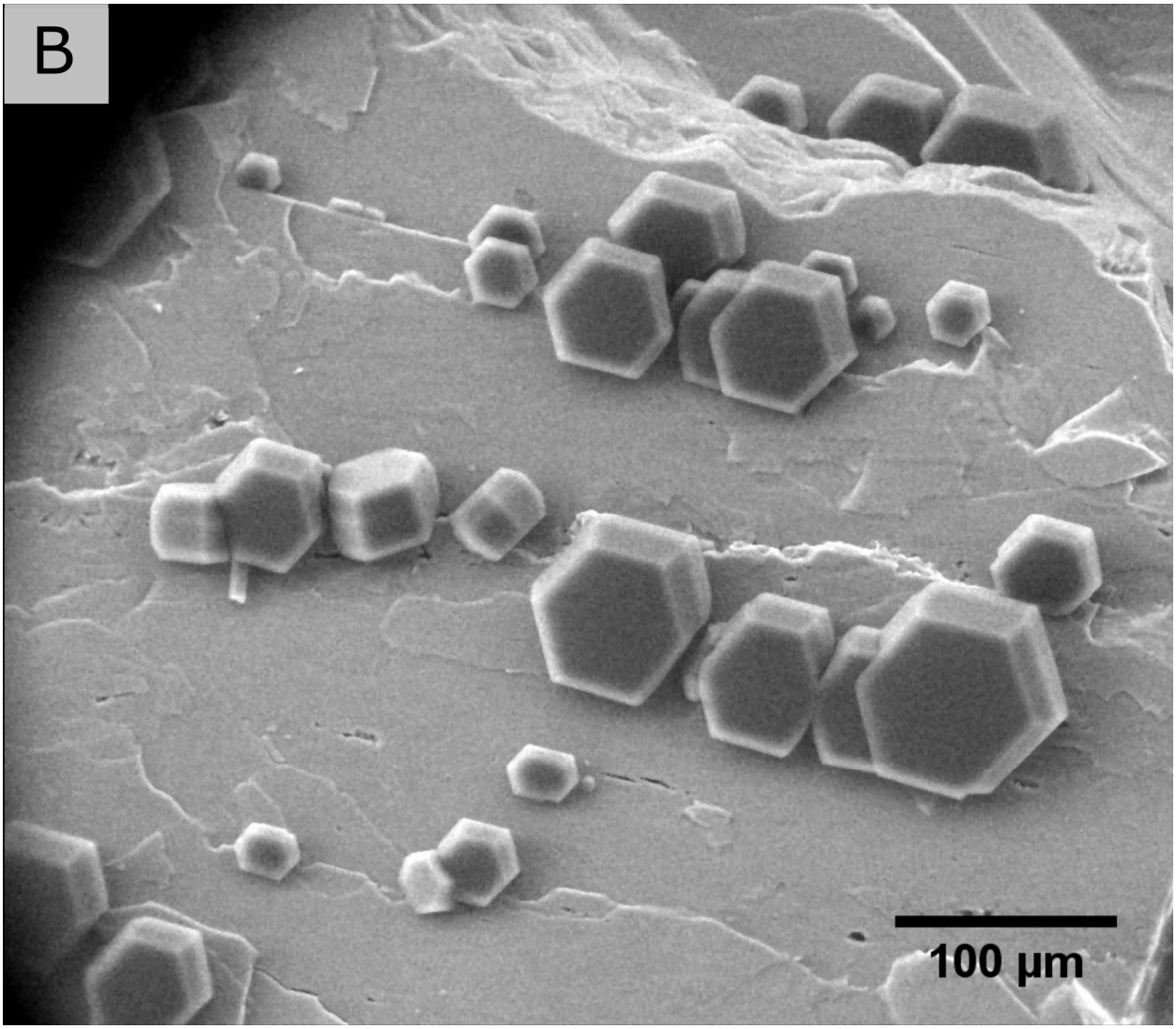

Figure 2B

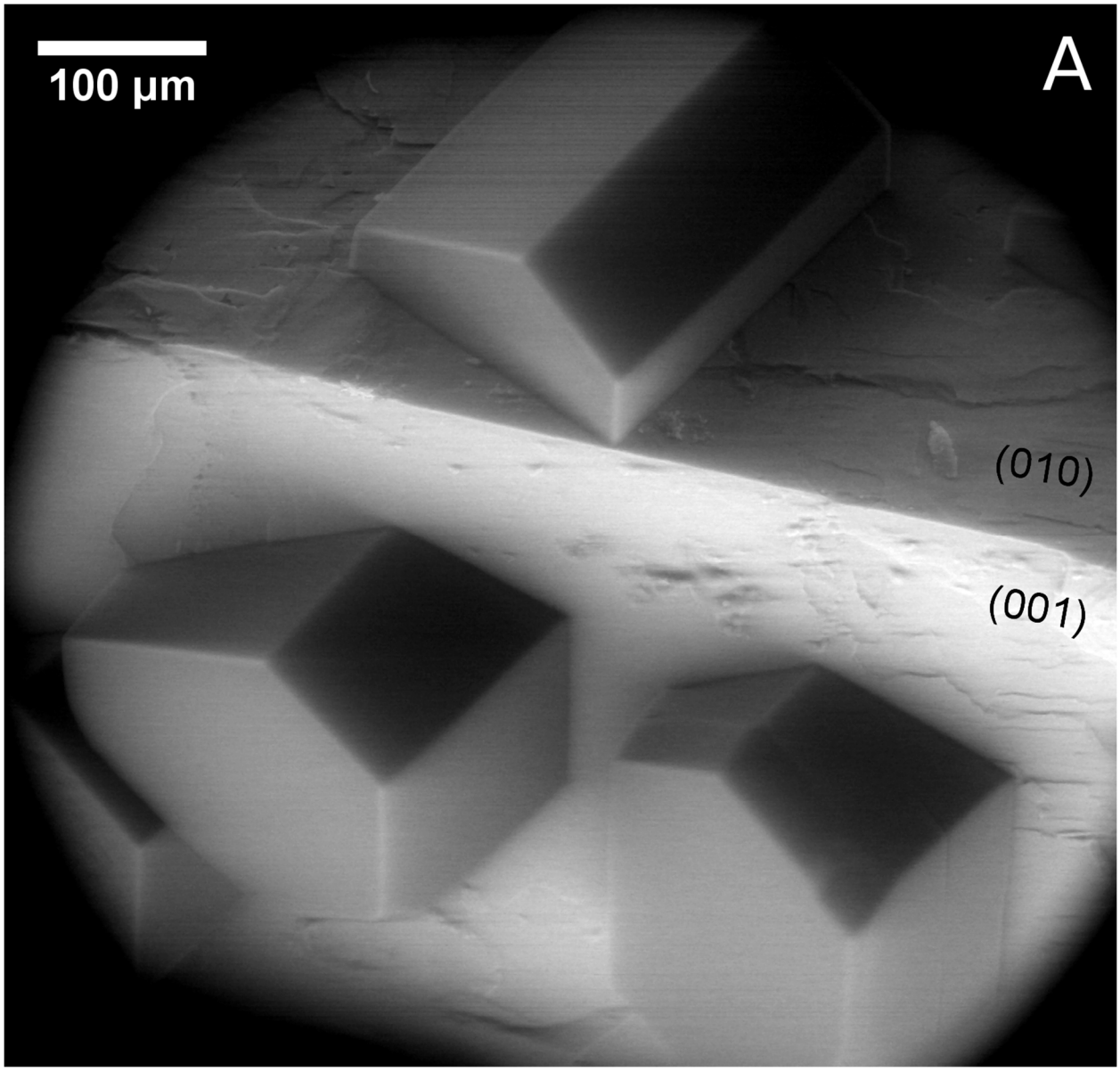

Figure 3A

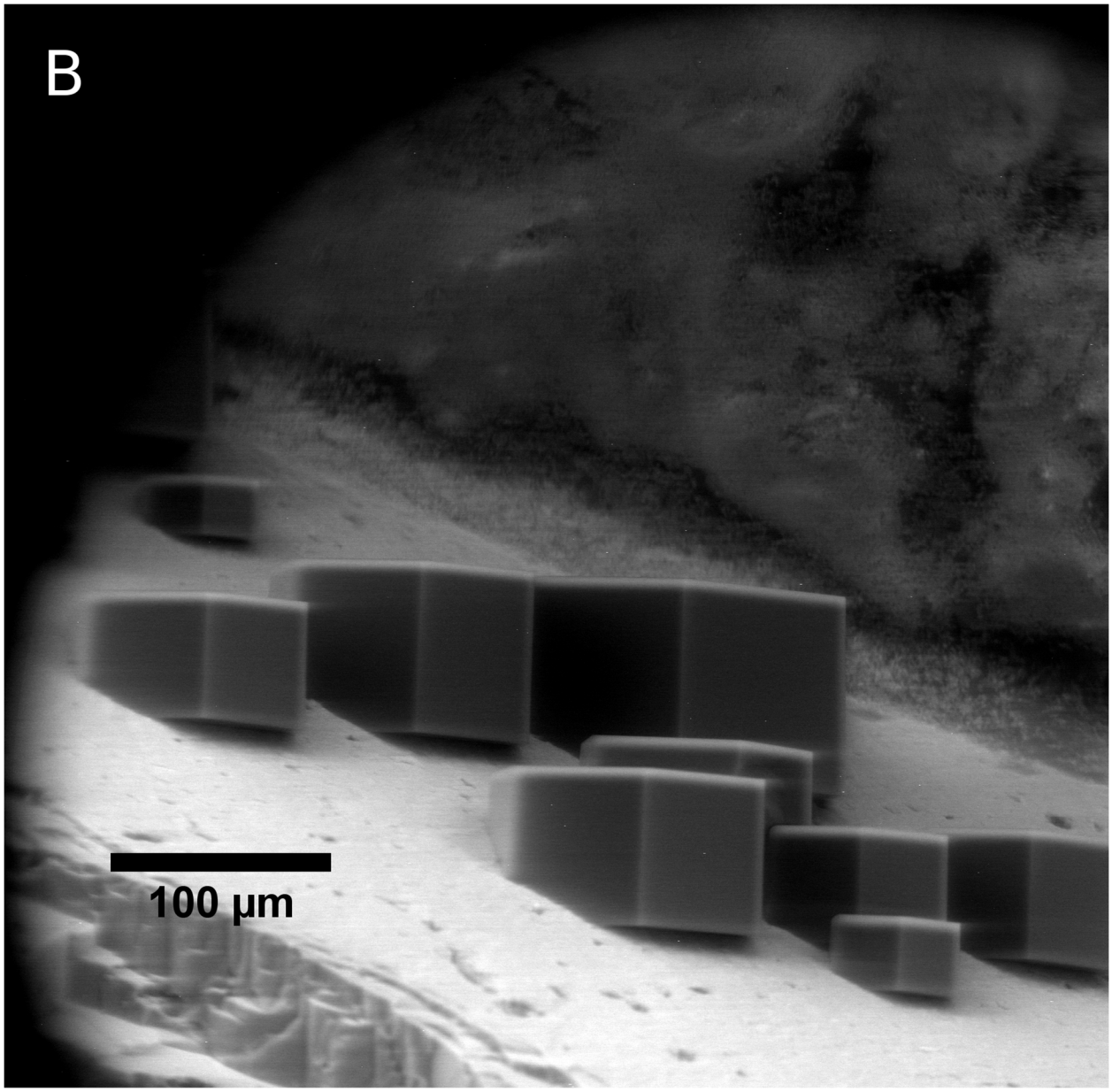

Figure 3B

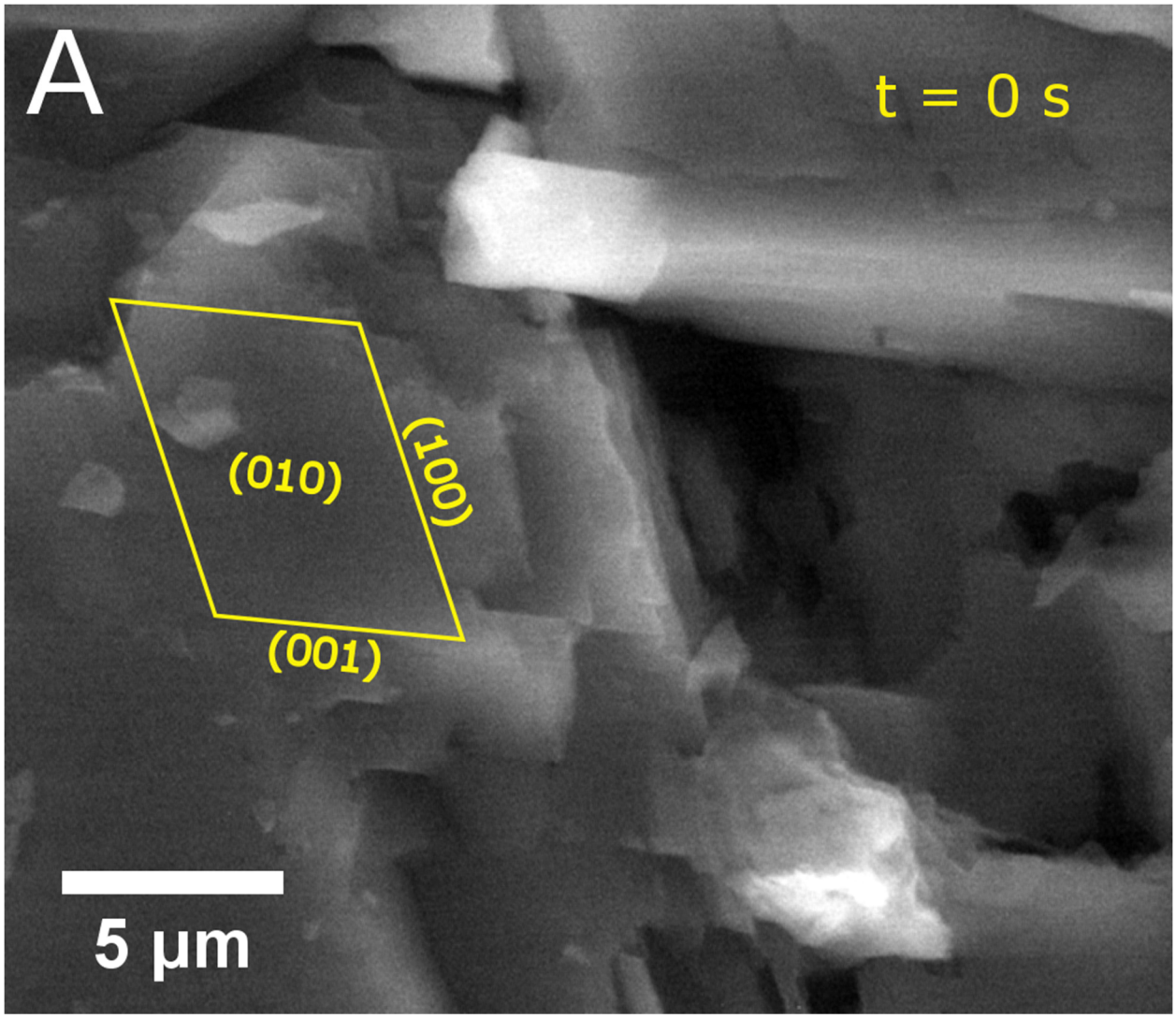

Figure 4A

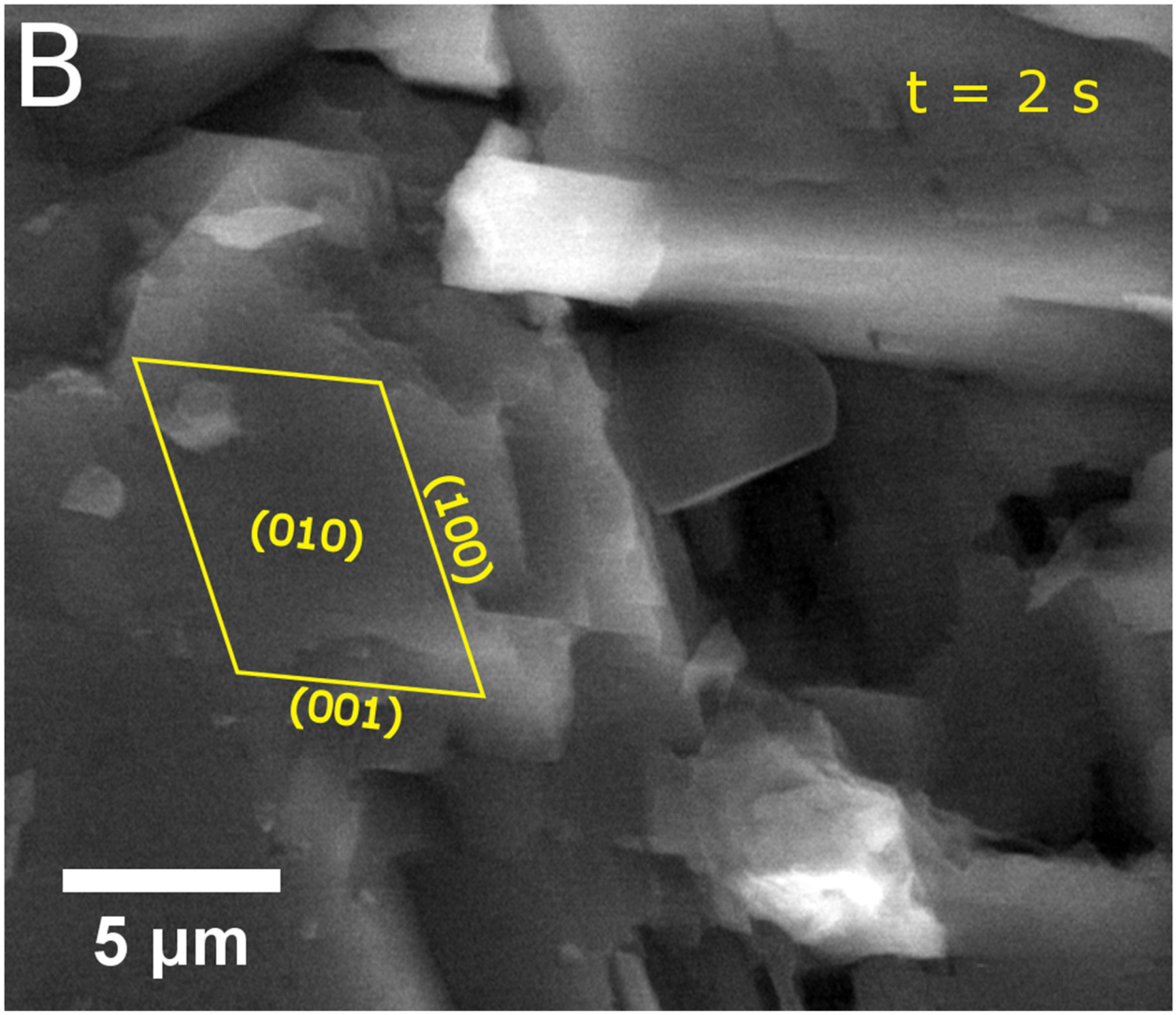

Figure 4B

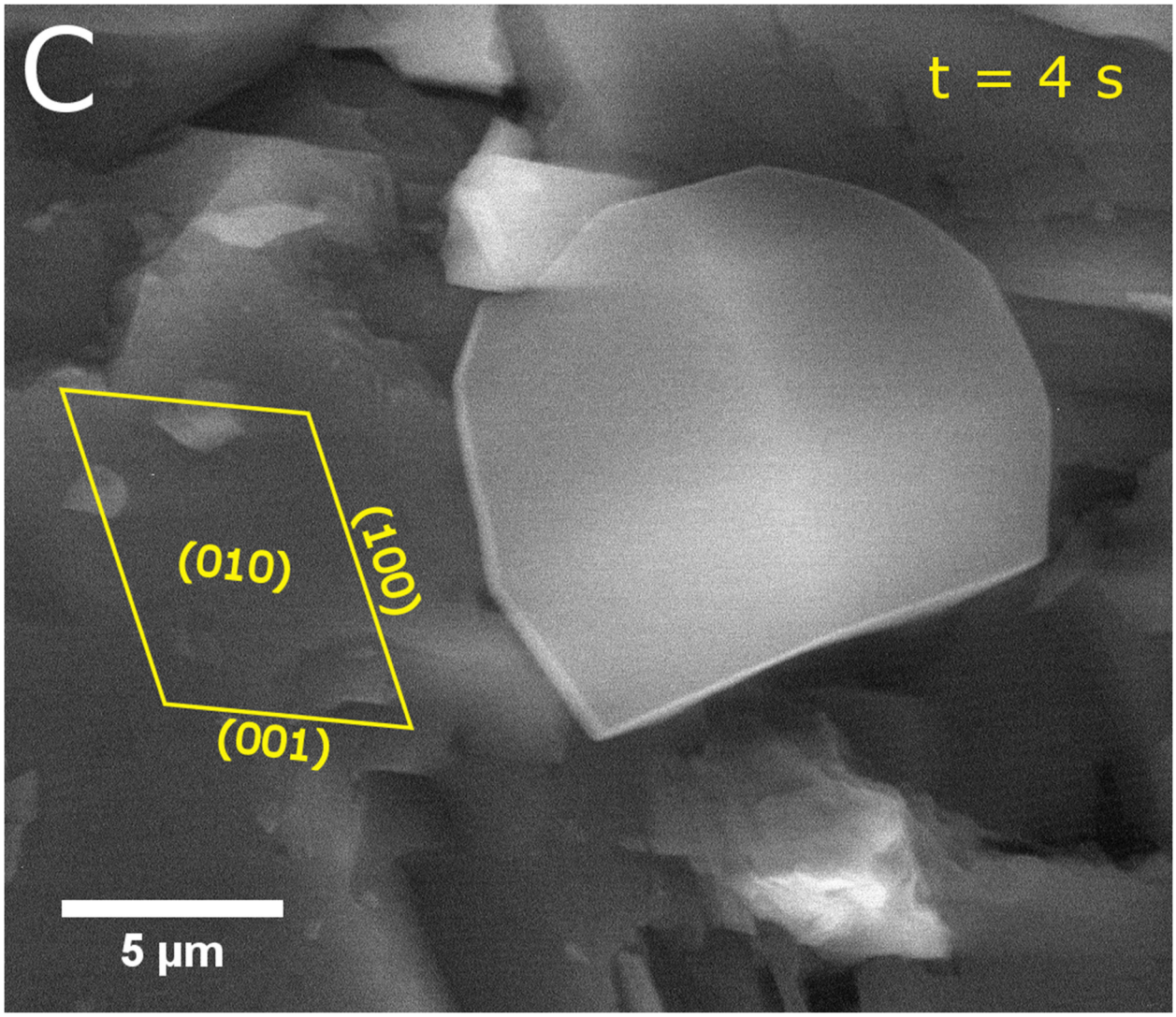

Figure 4C

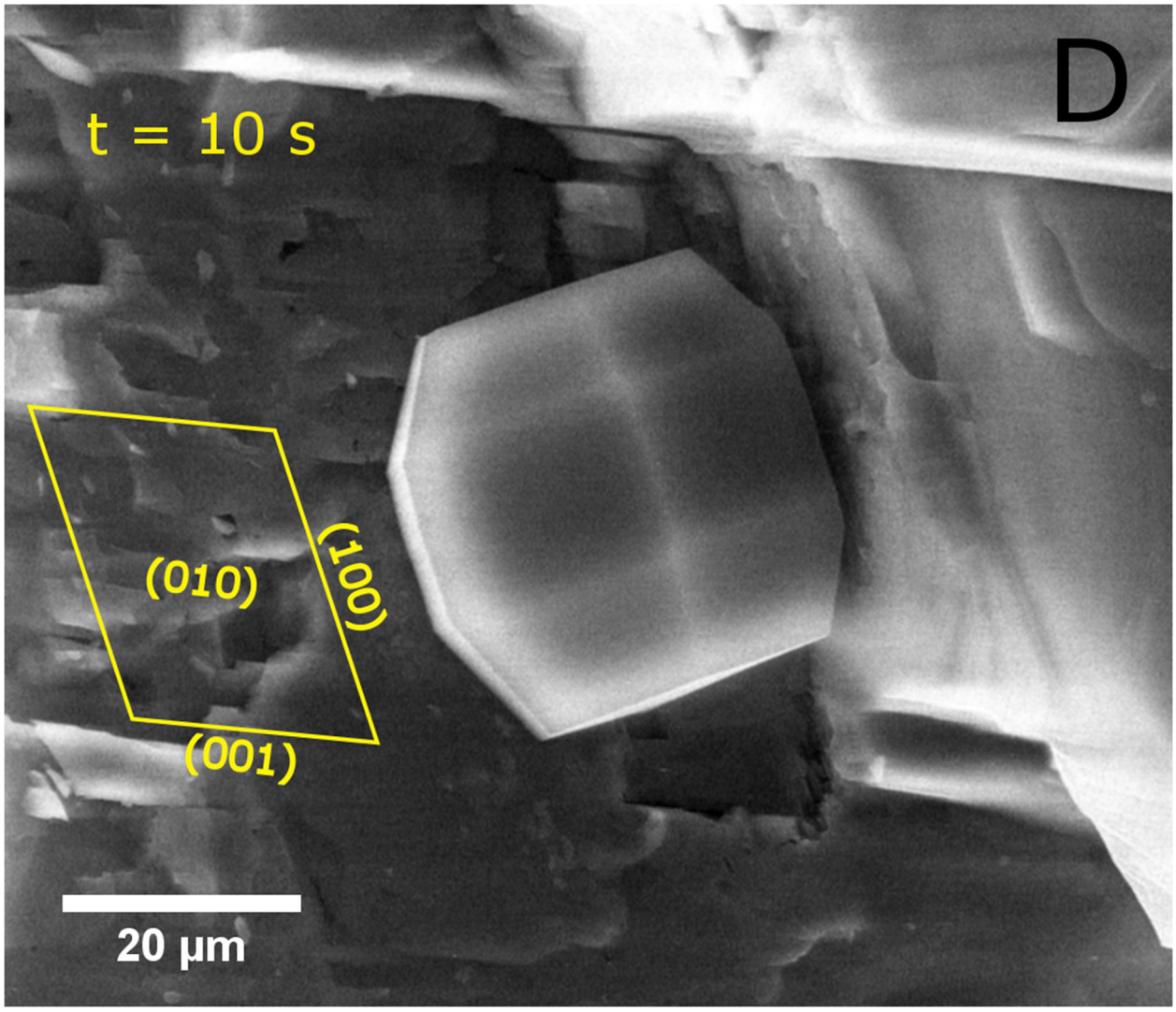

Figure 4D

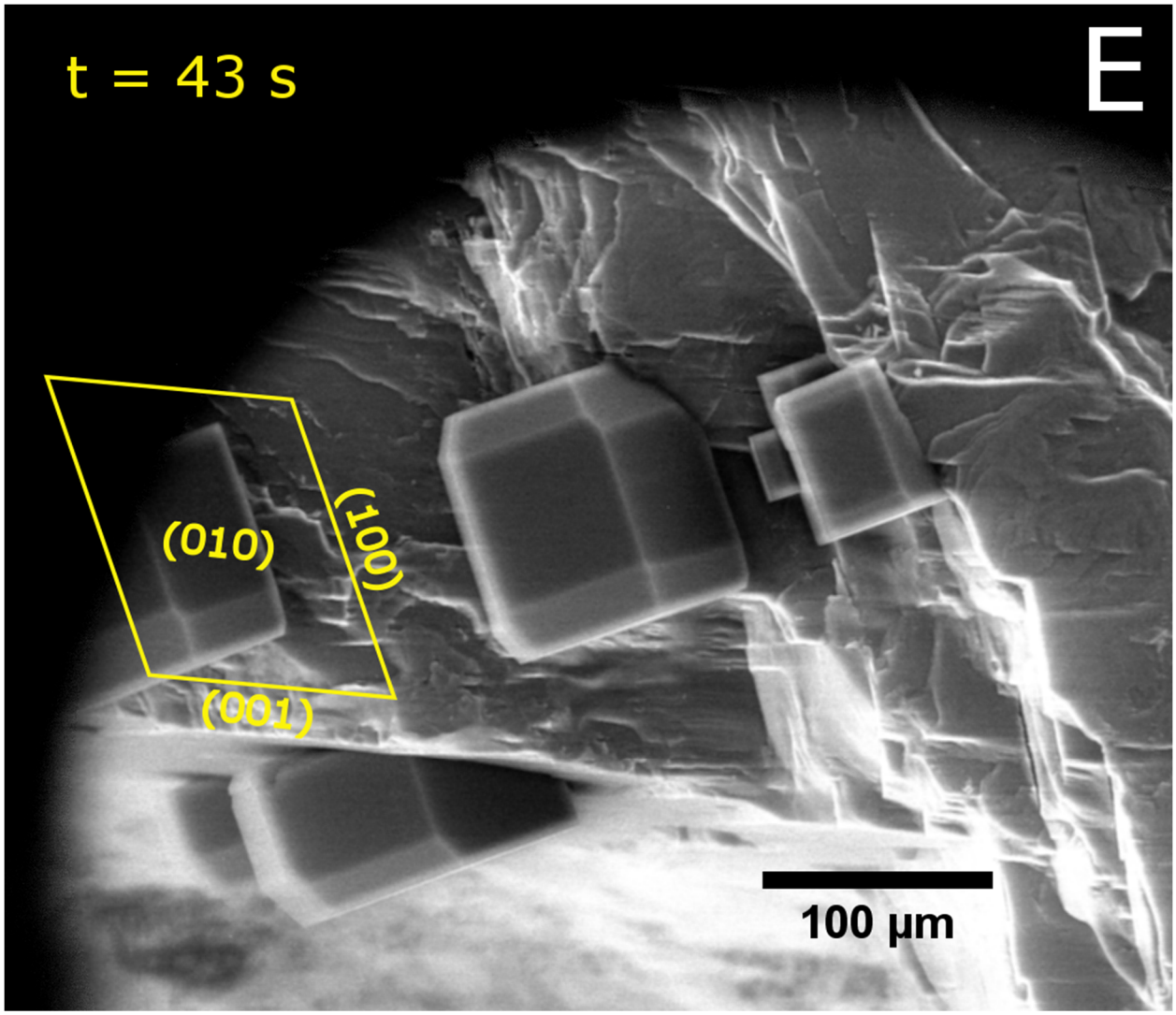

Figure 4E

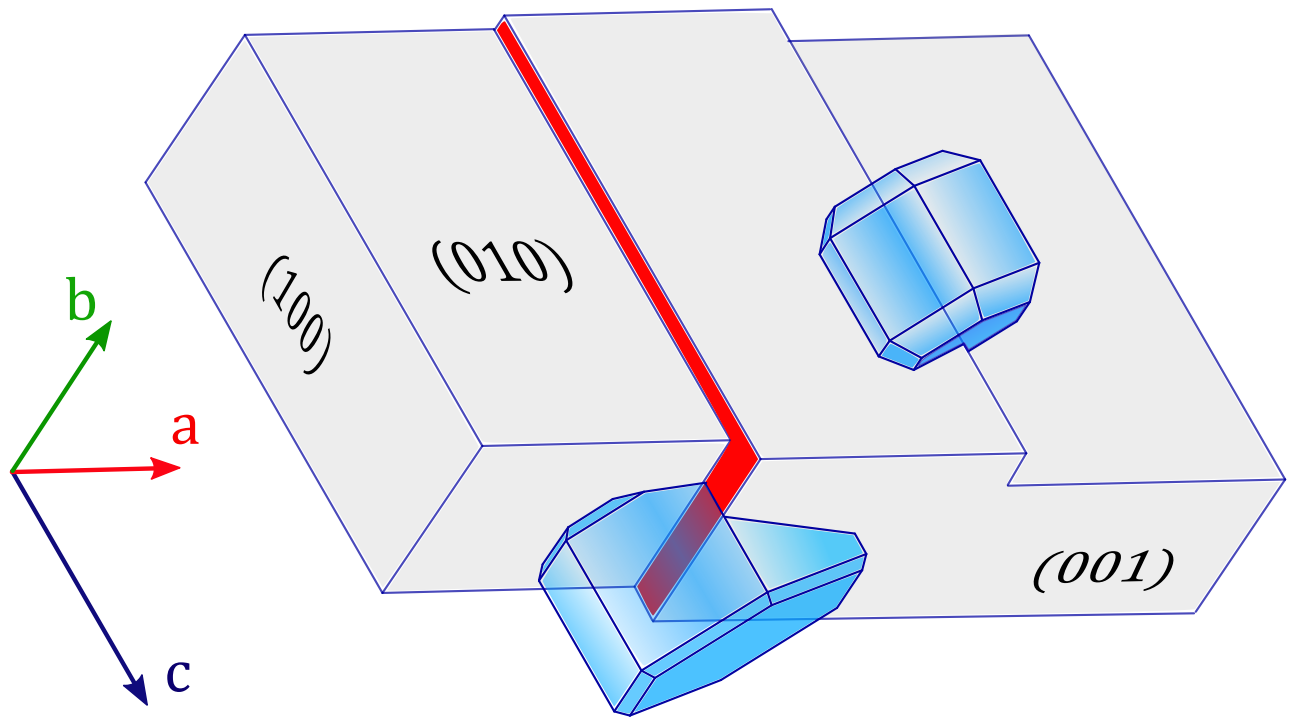

Figure 4F

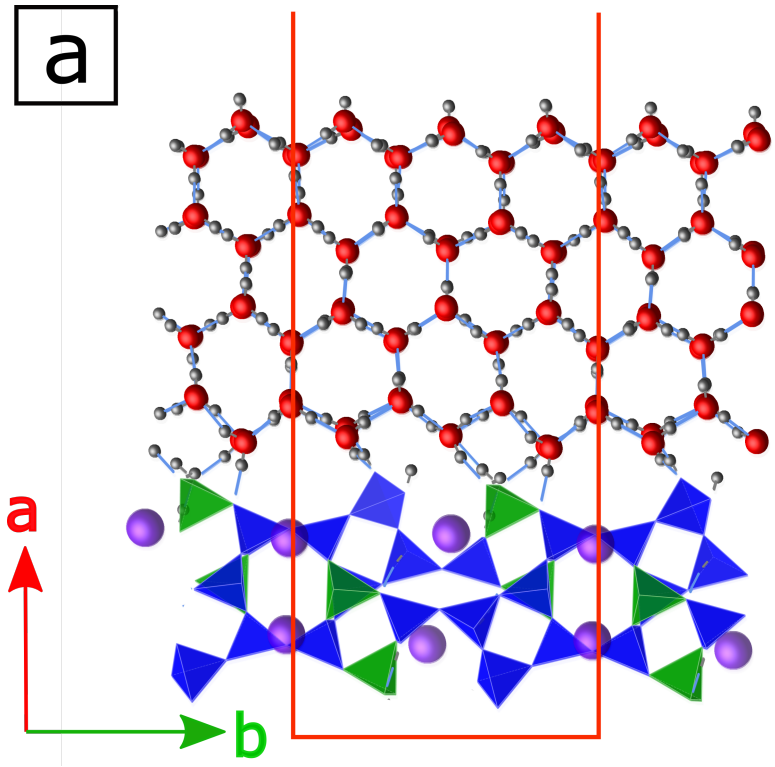

Figure 5A

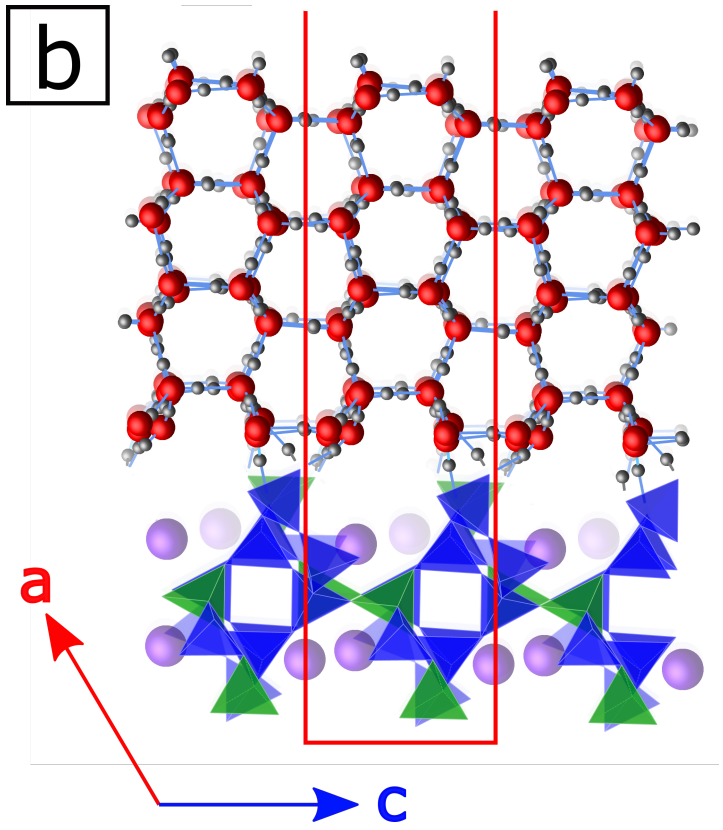

Figure 5B

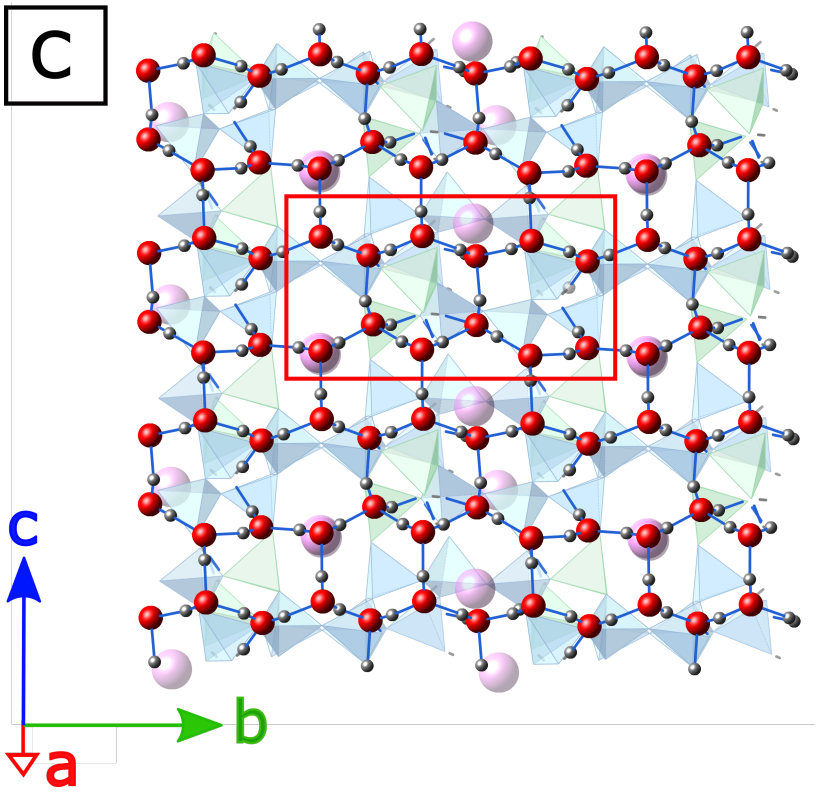

Figure 5C